COMPUTATIONAL METHODS FOR TWO-DIMENSIONAL AND THREE-DIMENSIONAL INLETS IN SUBSONIC AND SUPERSONIC FLOW*

J. Grashof and W. Schmidt
Theoretical Aerodynamics, Dornier GmbH
Friedrichshafen, F.R.G.

Abstract

In the present theoretical investigations Pitot-inlets are studied in subsonic and supersonic flow. Several theoretical methods have been developed. They have in common that the full time-dependent Euler equations written in integral-conservation form are solved applying a finite-volume approach. Two-dimensional, axisymmetric and three-dimensional configurations are treated. For subsonic flow the computational grids are stationary, however, for supersonic free stream the grids are time-dependent and aligned to the bow-shock ahead of the inlet. Several space and time discretization techniques have been applied and analyzed in detail, e.g. MacCormack and Runge-Kutta-time stepping. Some results are shown and compared to other theoretical results and to experimental data.

I. Introduction

The efficiency of modern aircrafts depends to a large extend on the engine characteristics, which are essentially influenced by the inlet performance. The purpose of the inlet is for a broad spectrum of flight conditions to recompress the free stream to a prescribed pressure in the compressor entrance plan. An optimal inlet should yield maximum pressure recovery, minimum drag-including spillage drag-, and minimum flow distortion in the compressor entrance plane for the design situation. In addition, in "off-design"-maneuvers the air-intake system should provide good pressure recovery and flow quality. The so-called Pitot-inlets show some favourable properties, also with respect to fabrication and operation. Therefore, this type of inlets has been chosen for detailed numerical and experimental investigations. The computational methods presented have been developed within the past five years with the definite purpose to support the inlet designer in his difficult work and to avoid serious mistakes as early as possible. The theoretical investigations have started with the development of computational methods for two-dimensional or axisymmetric supersonic inlets. After some experiences these methods have been extended to three-dimensional cases. At present, the related work for inviscid three-dimensional subsonic air-intakes has been completed. The time-dependent Euler equations written in integral-conservation form are solved by the finite-volume approach, thus avoiding special treatment of flow discontinuities (e.g. shocks) and allowing computational grids which need not be differentiable. Since the studies concentrate on the detailed properties of the inlet-lip region, only isolated inlets have been treated in the past, i.e. the presence of fuselage, splitter plate etc. is neglected or sometimes replaced by an appropriate symmetry condition. Related examples will be presented below. Ongoing efforts include the actual fuselage shape and wing.

* The investigations have been partially supported by the German Ministry of Defence under RüFo4 contracts.

II. Computational domain and mesh generation

The boundary of the computational domain has to be chosen in such a manner that accurate boundary conditions can be formulated on each segment of the boundary. Naturally, the body surface and the exit cross-section of the inlet channel are parts of the boundary. For special cases (e.g. axisymmetric flow) the symmetry axis of the flow is a further part of the boundary. The computational domain is closed by the far-field boundary, its location depending fundamentally on the free-stream condition:

Subsonic free stream

The far-field boundary has to be located far away from the body. The computational mesh is constructed on the basis of the complex Maxwell-transformation[1]

$$z = \frac{a}{\pi}\,(w+1+e^{w}) \qquad (1)$$

with $z = x + iy$, $w = u + iv$ (2)

The curves u = const and v = const are shown in Fig. 1 for the case of an inlet with zero thickness. The three-dimensional mesh is composed by a set of two-dimensional grids of Maxwell type. The two-dimensional grid generation is performed as follows:

Discretize the body contour, the exit section and the x-axis in an appropriate manner and compute the related values w by an iterative inversion of equ. (1); discretize u and v (stretching) in the intervalls u (body) to u (axis) and v (body) to v (axis) and get thus the transformed grid u(i,j), v(i,j); the grid points are counted by indices i,j forming the integer space. Improve the transformed grid by solving a set of geometric Poisson-equations in the transformed plane w and transform back to the physical plane z using equ. (1). A sample of the final grid is depicted in Fig. 2. This provides a "high-quality" computational grid for inlet-flow calculations.

Remark: This method for grid generation seems to be new and can analogously be applied to other configurations (e.g. blunt-body flow etc.). For clarity it is noted that this procedure has nothing in common with conformal mapping.

Supersonic free stream

The far-field boundary has to enclose the subsonic flow region. It is build up by the inner part of the bow-shock surface (inflow boundary) and a plane downstream of the outer subsonic flow region[2]. The mesh is again composed by a series of sectional grids which are constructed by interpolation of a family of ray (i = const) from the body surface to the shock and - for the channel region - from the body to the axis (Fig. 3). Since the mesh is shock-aligned, it is changed with time according to the travelling of the shock wave. The spatial location of the rays is changed only for those rays which hit the x-axis. At the beginning of a flow computation some skill is necessary to construct an initial grid which will enclose the subsonic flow for all times.

III. Basic equations in integral-conservation form

The Euler equations including the energy equation may be written in brief notation for a mass-attached control volume V(t) (see e.g. Ref. 3):

$$\int_{V(t)} \frac{\partial}{\partial t} \vec{U}\, dV + \int_{S(t)} \bar{\bar{H}}\, d\vec{S} = 0 \qquad (3)$$

$\vec{U}$ is a formal vector and $\bar{\bar{H}}$ a formal flux tensor. The finite-volume method works on the basis of a cartesian coordinate system:

Space vector: $$\vec{r} = x \cdot i_x + y \cdot i_y + z \cdot i_z \qquad (4)$$

Velocity vector: $$\vec{q} = u \cdot i_x + v \cdot i_y + w \cdot i_z \qquad (5)$$

Then the formal vector $\vec{U}$ and the formal flux tensor $\bar{\bar{H}}$ become

$$\vec{U} = \begin{bmatrix} \rho \\ \rho u \\ \rho v \\ \rho w \\ e \end{bmatrix}, \quad \bar{\bar{H}} = \begin{bmatrix} \rho \cdot \vec{q} \\ \rho u \cdot \vec{q} + p \cdot i_x \\ \rho v \cdot \vec{q} + p \cdot i_y \\ \rho w \cdot \vec{q} + p \cdot i_z \\ (e+p) \cdot \vec{q} \end{bmatrix} \qquad (6)$$

Nomenclature: t = time, V = volume, S = surface of V, dV = element of V, $d\vec{S}$ = outer area vector of surface element dS, ρ = density, p = pressure, e = total energy per volume unit.

The set of basic equations is completed by an equation of state (ideal gas):

$$p = (\gamma - 1) \cdot \left[e - \frac{1}{2} \rho \cdot (u^2 + v^2 + w^2) \right] \qquad (7)$$

with γ = ratio of specific heats.

This system of equations holds also for control volumes fixed in space.

For control volumes neither mass-attached nor fixed in space (i.e. general time-dependent volumes) equ. (3) has to be replaced by

$$\frac{d}{dt} \int_{V(t)} \vec{U}\, dV + \int_{S(t)} \bar{\bar{H}}\, d\vec{S} - \int_{S(t)} \vec{U} \cdot \vec{\lambda}\, d\vec{S} = 0 \qquad (8)$$

Here, $\vec{\lambda}$ is the shift-velocity vector of dS. These general equations are simply reduced to two-dimensional cases, however, the axisymmetric formulation shows some differences[4]:

$$\frac{d}{dt} \int_{V(t)} \vec{U}\, dV + \int_{S(t)} \vec{U} \cdot (\vec{q} - \vec{\lambda})\, d\vec{S} + \int_{S(t)} \vec{P}\, d\vec{S} + \int_{V(t)} \vec{E}\, dV = 0 \qquad (9)$$

with

$$\vec{U} = \begin{bmatrix} \rho \\ \rho u \\ \rho v_r \end{bmatrix}, \quad \vec{P} = \begin{bmatrix} 0 \\ p \cdot i_x \\ p \cdot i_r \end{bmatrix}, \quad \vec{E} = \begin{bmatrix} \rho \\ \rho u^2 \\ \rho u v_r \end{bmatrix} \qquad (10)$$

(v_r = radial component of $\vec{q}$, i_r = radial unit vector).

The flow computations for supersonic inlets have been performed taking advantage of the reasonable assumption of total enthalpy h_T being constant with time[4]. The energy equation is omitted and the pressure is calculated from

$$p = \frac{\gamma - 1}{\gamma} \cdot \rho \cdot \left[h_T - \frac{1}{2} (u^2 + v^2 + w^2) \right] \qquad (11)$$

and $$h_T = \frac{\gamma}{\gamma - 1} p_o / \rho_o + \frac{1}{2} (u_o^2 + v_o^2 + w_o^2) \qquad (12)$$

Index o indicates free-stream conditions. The assumption h_T = const is justified for the present class of flow problems in which only the steady state is of interest ignoring the transitorial behaviour. The computational expense is reduced remarkably, however, during the studies of three-dimensional supersonic inlet flows one disadvantage of the assumption h_T = const became apparent: The compatibility relations (characteristic relations), which can be used to calculate the bow-shock velocity, switch over to a very complicated form[5] (in contrast to the related form without h_T = const which remains very simple, even in the three-dimensional case).

IV. Initial- and boundary conditions

Initial conditions

Subsonic free stream:

The computation is started from scratch, i.e. in the whole computational domain the undisturbed flow quantities are prescribed.

Supersonic free stream[2]*:*

For brevity the two-dimensional case is outlined. First step: Calculate the flow quantities behind the bow-shock (oblique stationary shock) for each cell of the shock surface. Second step: On the rays i = const between shock surface and body surface the density ρ is set equal to the density $\rho_s(i)$ behind the shock; the velocity is interpolated linearly in j on the rays i = const whereby the condition of zero normal velocity on the wall is incorporated. The pressure field is calculated from the density- and velocity fields using the condition of constant total

enthalpy, eq. (11). Third step (channel region): at the exit plane parallel outflow is assumed ($v = 0$, $w = 0$); the pressure is interpolated linearly in i between shock and channel exit. The density is computed from the pressure field assuming isentropy. Finally the velocity field is approximated taking into account the condition h_T = const and again the condition of zero normal velocity at the wall.

Boundary conditions

Improper treatment of boundary conditions can lead to serious errors and perhaps instability[6]. The fundamental idea how to formulate properly posed boundary conditions is based on the analysis of disturbance propagations at the boundaries, i.e. on the distinction between incoming and outgoing characteristics. For instance, numerical "error waves" should be absorbed at a boundary or they should travel out of the computational domain instead of being reflected. These principles are strictly taken into account in the numerical methods for inlet-flow analysis, see references (2), (4), (6), (7). Instead of going into details we restrict ourselves on two special points:

Boundary conditions at channel exit:

All calculations have been carried out for subsonic flow condition at the channel exit. Parallel stream is assumed and the static pressure p_{ex} is prescribed. The flow quantities are then calculated by solving locally the basic flow equations in conservation form[2].

Bow-shock velocity[2],[7]*:*

In principal there are two possibilities to calculate the velocities of the bow-shock panels:

(a) implementation of characteristic relations[8]

(b) extrapolation of appropriate flow quantities (e.g. pressure) from inside of the computational domain to the rear side of the shock surface and local application of the usual shock relations.

For two-dimensional or axisymmetric cases both versions have been applied and the results were nearly identical. For three-dimensional configurations the characteristic relations become very complicated[5] due to the condition h_T = const. In principle, it is evident how to incorporate these relations to calculate the shock velocity, however, some studies have shown that the version (a) would become very expensive (note that one has to work in four-dimensional space). Therefore version (b) has been chosen, and the related results were quite satisfactory.

V. Numerical solution of the basic equations

During the development of the computational methods for inlet-flows continuous efforts have been spent on improvement of the algorithms with respect to accuracy, convergence rate and stability limits. Instead of describing this evolution by the related finite-difference equations it seems preferable to characterize verbally the stages of numerical algorithms used. Details may be found in the references cited. In chronological sequence these stages are:

(a) Supersonic two-dimensional or axisymmetric inlet flow

Method: explicit time-splitted predictor-corrector of MacCormack[9]. This well-known method has been applied formerly for instance by Rizzi and Inouye[3] for blunt-body calculations.

(b) Supersonic three-dimensional inlet flow

1. Method: no success with method (a)
2. Method: explicit predictor-corrector without time-splitting (i.e. without subsequent sweeps in the coordinate directions i,j,k) after MacCormack[9]. The method worked satisfactorily for the present case, but with poor convergence rate.
3. Method: explicit three-stage two-level Runge-Kutta time-stepping scheme[6]. The method uses central approximations to compute the fluxes at the volume faces (in contrast to MacCormack's schemes which use a sequence of one-sided approximations). The three-stage method is more accurate in time and faster than method (b.2), since it is stable for CFL ≤ 2 (CFL = Courant/Friedrich/Lewy number). In addition numerical dissipation is added by a Shuman-type filter which preferably removes high-frequency numerical disturbances.

(c) Subsonic three-dimensional inlet flow

Method: explicit four-stage two-level Runge-Kutta local time-stepping with filtering and enthalpy forcing term[6]; further improvement of method (b.3). Since the mesh does not change with time, the computational expenditure is reduced remarkably in comparison with case (b).

VI. Results for supersonic free stream

Axisymmetric configurations

Some of the results have already been published[4]. For the NACA-inlet IC the computed wall pressure is shown in Fig. 4 and is compared with a numerical solution of the full potential equation written in non-conservative form[10]. In spite of the relatively coarse grid used for the present method the results compare well with both the prediction of Arlinger[10] and the experiment[11]. For the same inlet the bow-shock distance vs. mass-flow ratio is presented in Fig. 5. The predicted distances are slightly smaller than the measured ones and the discrepancy decreases with increasing mass-flow ratio. For additional results see references (2) and (4).

Three-dimensional kidney-shaped inlet

A front view of the inlet EM1[2] is shown in Fig. 6 together with the sections A through G, where pressure measurements have been performed[12],[13]. The numbers 1 through 17 indicate the sections k of the three-dimensional computational mesh. Since AG is a symmetry plane most of the calculations have been carried out for a "half inlet" imposing symmetry conditions along AG. For a free-steam Mach number of Mo = 1.46, incidence $\alpha = 0$ and pressure ratio $p_{ex}/p_o = 2.30$ the numerical results (wall pressure, computational mesh, sonic line) are shown in Fig. 7. Fig. 8 presents the cross-flow in the fictitious channel-exit plane (internal boundary). A reasonable comparison with experimental results[12],[13] is only pos-

sible in the lower range of the inlet, since the theoretical prediction neglects the fuselage (isolated inlet body). The theoretical and experimental pressure distributions are compared for the side section D (k = 5) (Fig. 9.a) and for the lowest lip section G (k = 9) (Fig. 9.b). There are only minor differences between theory and experiment which may be ascribed to the assumption "isolated inlet".

VII. Results for a subsonic three-dimensional inlet

For the inlet depicted in Fig. 10 a series of flow computations has been performed. Some results for two cases are discussed below:

(a) $M_o = 0.80$, $\alpha = 0^o$, $p_{ex}/p_o = 1.3270$, $\varepsilon_{HL} = 0.60220$

(b) $M_o = 0.80$, $\alpha = 6^o$, $p_{ex}/p_o = 1.3270$, $\varepsilon_{HL} = 0.66700$

Here ε_{HL} is the mass-flow ratio with respect to the high-light area A_{HL}: $\varepsilon_{HL} = A_o/A_{HL}$. Note, the ε_{HL}-values are not prescribed but are computed from the final result of the flow calculation. Again, an isolated inlet is assumed and the fuselage respectively the splitter-plate is replaced by a symmetry condition. A part of the grid in this symmetry plane is shown in Fig. 10. The three-dimensional grid is composed by 17 two-dimensional grids of Maxwell-type; wall pressures are measured in 5 sections, see Fig. 11.

Experimental cases for comparison with (a) and (b):

(α) $M_o = 0.75$, $\alpha = 0^o$, $\varepsilon_{HL} = 0.606$

(β) $M_o = 0.80$, $\alpha = 6^o$, $\varepsilon_{HL} = 0.652$

The computational results (e.g. wall pressure) are stored in the volume centers; therefore a direct comparison is possible only for

- numerical results for k = 6 with experiments at station 2,
- numerical results for k = 12 with experiment at station 4.

A similar comparison at the remaining pressure-hole sections would need a three-dimensional interpolation of the theoretical values; that is a difficult task for the present geometry and has not been done here. Hence, the comparison with experimental values at stations 1, 3 and 5 is more or less of qualitative nature. An additional difficulty stems from slight differences in the values for M_o and ε_{HL}.

Case (a) is compared to experiment (α) in Fig. 12 and (b) to (α) in Fig. 13.

Discussion

In all cases the experimental pressure distributions are predicted fairly well in the channel region and near the inlet nose. This fact is not remarkable since the predicted mass-flow ratio and the experimental one are nearly the same. However, a pronounced discrepancy is observed for the side sections of the inlet, e.g. at k = 6,9,12. Here the suction peaks are underpredicted by the computation. This can be explained by the influence of the fuselage of the wind-tunnel model on the flow in front of the inlet. The fore-body has a conical shape, approximately, and distorts the free stream to a divergent flow. Hence, in contrast to the numercial analysis, the inlet body experiences an inhomogeneous oncoming flow field similar to a yaw angle, i.e. at the side sections of the inlet a lateral incidence is induced by the fore-body. A qualitative evidence of this explanation will be given below:

The evaluation of a numerical potential-flow solution of the three-dimensional wing-body combination at $M_o = 0.76$ and $\alpha = 0^o$ indicates, that the fore-body displaces the stream lines by about 5 degrees in lateral direction corresponding to the position k = 9 of the inlet. If the above explanation would hold, the suction-peak differences should vanish in the comparison of the theoretical pressure distributions with related experimental data measured at a yaw angle $\beta = -5^o$. Unfortunately, no experiments for $\beta = -5^o$ are available. Therefore, an experimental result for $\beta = +5^o$ is taken:

(γ) $M_o = 0.75$, $\alpha = 6^o$, $\beta = 5^o$, $\varepsilon_{HL} = 0.648$

Since in (γ) the yaw is just in the opposite direction it is expected that the suction-peak differences shown in Fig. 13 will be duplicated at the side sections whereas these differences remain approximately unchanged for the inlet sections near the fuselage. This conjecture is indeed substantiated, see Fig. 14. So this last study has proven the explanation given above: The mentioned pressure-peak discrepancies between theory and experiment (shown in Fig. 12 and Fig. 13) are caused by the fore-body of the wind-tunnel model which induces a yaw effect upon the air-intake; obviously, this can't be modelled by the present calculation for an isolated inlet.

The inlet body has been designed under the constraint that the flow should be shockless in the design situation. Inspection of the theoretical results shows that this goal has been achieved, i.e. the supersonic regions depicted in Fig. 15 and Fig. 16 are not terminated by a shock.

Evidently a lot of further results, e.g. iso- and cross-flow plots, vector plots etc., could be presented to give more insight into the flow field; however, this is impossible within the frame of this paper.

VIII. Final remark

It has been outlined that the numerical methods to analyze subsonic and supersonic inviscid flows around isolated inlets are a useful tool for the design engineer. Meanwhile, from the comparisons with experimental data it is recommended to extend the investigations presented here to more complicated configurations, e.g. inlet with forebody, ramp, fuselage etc. including viscous effects. Related studies are now under work.

IX. References

(1) J. Grashof: Inlet mesh generation by using a Maxwell transformation, Dornier-Note, 1982.

(2) J. Grashof, W. Schmidt, A.W. Rizzi: Verfahren zur Berechnung der reibungsfreien Strömung an Überschalleinläufen, Dornier-Report 80/44B, 1980

(3) A.W. Rizzi, M. Inouye: Time-split finite-volume method for three-dimensional blunt-body flow, AIAA J., Vol. 11, 1973, pp. 1478-1485.

(4) A.W. Rizzi, W. Schmidt: Study of Pitot-type inlet-flow fields using the finite-volume approach, AIAA Paper 78-1115, 1978.

(5) J. Grashof: Charakteristikenbeziehungen für die dreidimensionalen, zeitabhängigen Euler-Gleichungen bei konstanter Gesamtenthalpie, Dornier-Note BF 30-1512/79, 1979.

(6) A. Jameson, W. Schmidt, E. Turkel: Numerical solutions of the Euler equations using Runge-Kutta time-stepping, AIAA Paper 81-1259, 1981.

(7) W. Schmidt, A. Jameson: Recent developments in finite-volume time-dependent techniques for two and three dimensional transonic flows, Von Kármán Institute for Fluid Dynamics, Belgium: Lecture Series 1982-04, March 29 - April 2, 1982.

(8) R.W. Porter, J.F. Coakley: Use of characteristics for boundaries in time-dependent finite difference analysis of multidimensional gas dynamics, Int. J. Numerical Methods in Engineering, Vol. 5, 1972, pp. 91-101.

(9) R.W. MacCormack, R.F. Warming: Survey of computational methods for three-dimensional supersonic inviscid flows with shocks, Advances in Numerical Fluid Dynamics, AGARD Lecture Series 64, Brussels, Belgium, 1973.

(10) B. Arlinger: Axisymmetric inlet flow at low supersonic Mach numbers, Symposium Transsonicum II, pp. 200-207, Springer-Verlag, 1975.

(11) W.B. Olstad: Transonic-wind-tunnel investigations on the effects of lip bluntness and shape on the drag and pressure recovery of a normal-shock nose inlet in a body of revolution, NACA RM L56C28, 1956.

(12) E. Wedemeyer, W. Schneider, G. Speckmann: Vorläufige Ergebnisse der Lippendruckmessungen am Modell EM1, DFVLR-AVA-Report IB 251-80 MB 03, 1980.

(13) H. Buers, D. Ritchie, H. Thiel, H. Welte, H. Zimmer: Überschalleinläufe - Experimenteller Teil, Abschlußbericht Phase I und Ia, Dornier-Report 80/17 B, 1980.

X. Figures

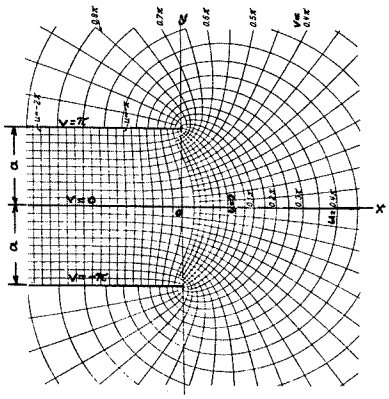

FIG.1: MAXWELL CURVES

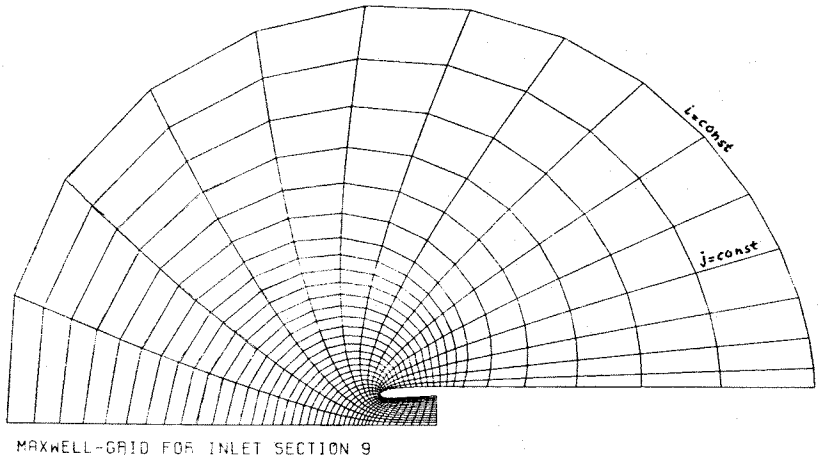

MAXWELL-GRID FOR INLET SECTION 9

FIG.2: GRID FOR SUBSONIC FREE STREAM

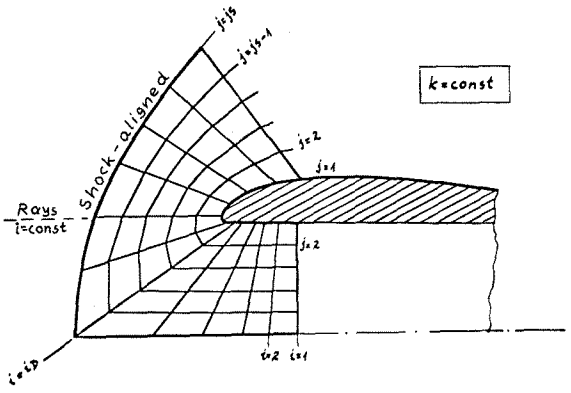

FIG.3: GRID FOR SUPERSONIC FREE STREAM

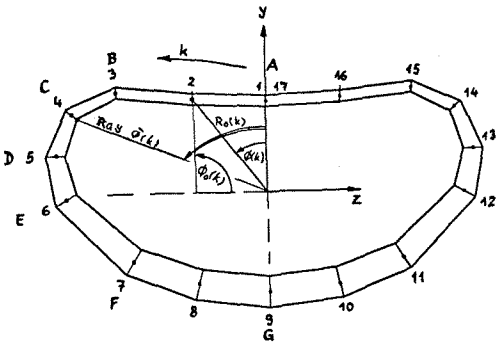

FIG.6: FRONT VIEW OF INLET EM1

A - G : PRESSURE-HOLE SECTIONS ,

K=1-17: GRID SECTIONS

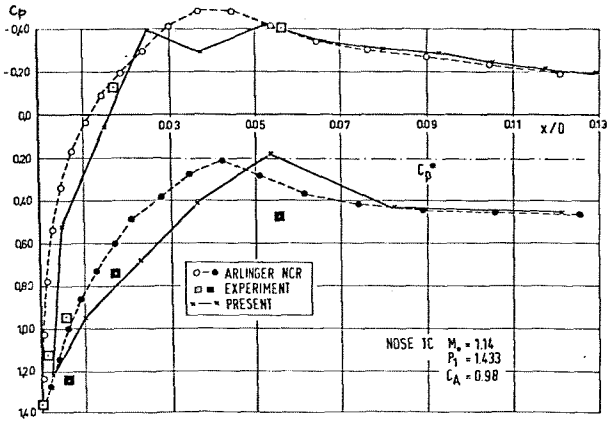

FIG.4: WALL-PRESSURE DISTRIBUTION FOR INLET IC

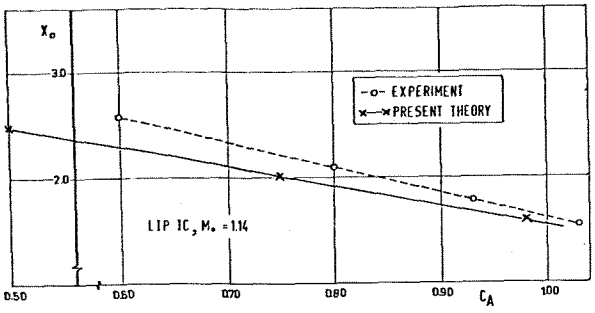

FIG.5: SHOCK DISTANCE VS. MASS-FLOW RATIO FOR INLET IC

FIG.7:

WALL-PRESSURE DISTRIBUTION , GRID AND SONIC LINE AT SECTION K , $M_o = 1.46$ $P_{ex}/P_o = 2.30$

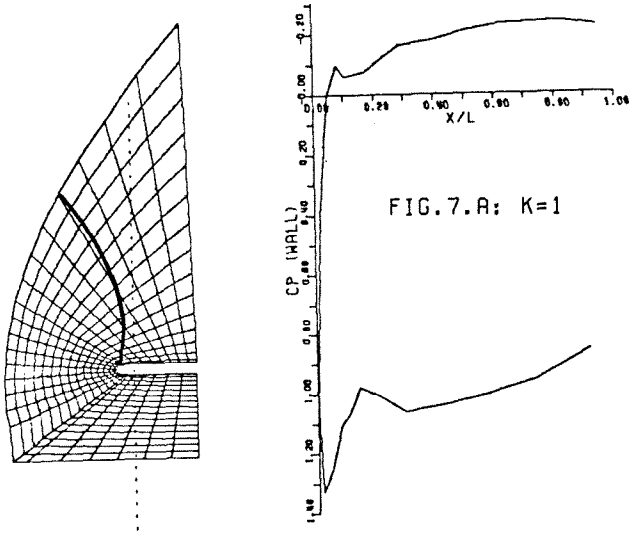

FIG.7.A: K=1

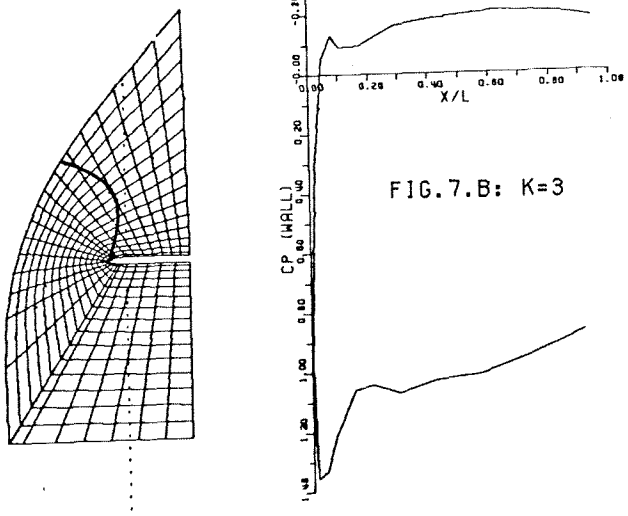

FIG.7.B: K=3

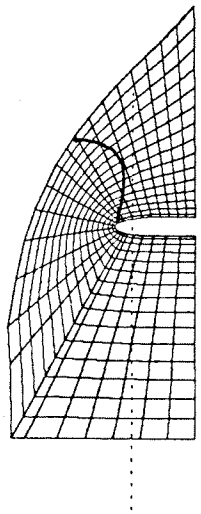

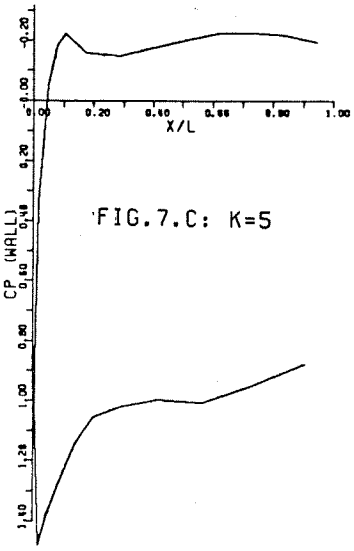

FIG.7.C: K=5

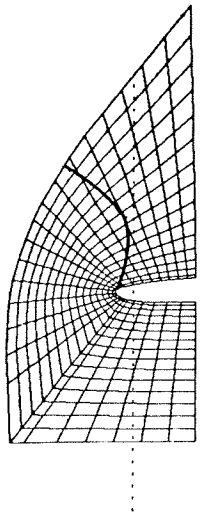

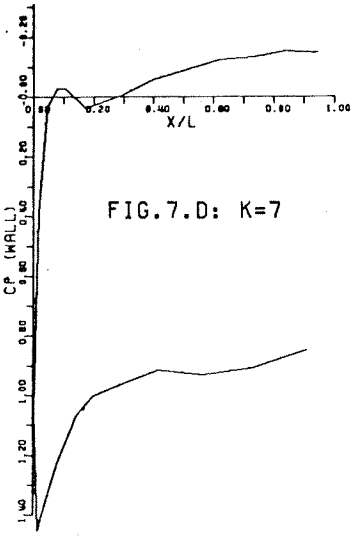

FIG.7.D: K=7

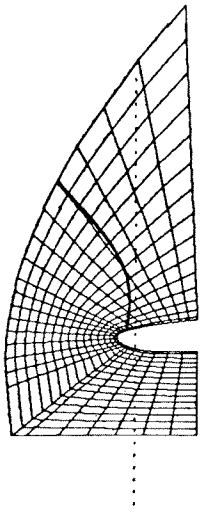

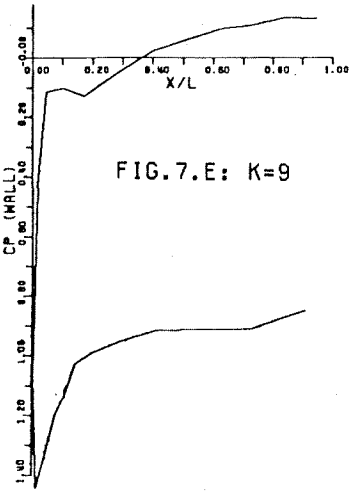

FIG.7.E: K=9

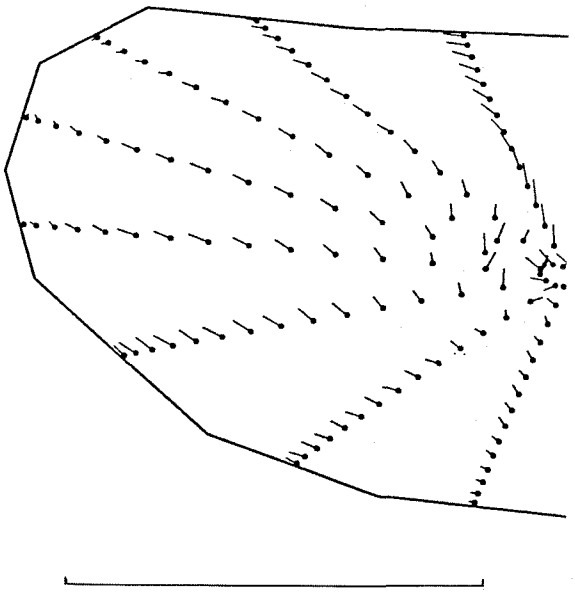

THIS LENGTH CORRESP. TO $(V^2 + W^2)^{1/2}/U=1$

FIG.8: CROSS-FLOW AT CHANNEL EXIT OF EM1 LIP.
$M_o=1.46$ $P_{ex}/P_o=2.30$

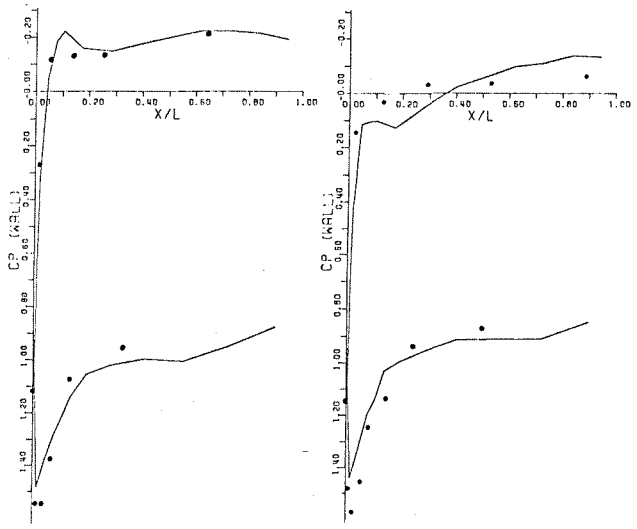

A: EM1 SECTION D (K=5) B: EM1 SECTION G (K=9)

FIG.9: WALL-PRESSURE DISTRIBUTION IN COMPARISON WITH EXPERIMENT, $M_o=1.46$ $P_{ex}/P_o=2.30$

● ● ● CP (EXPERIMENT)

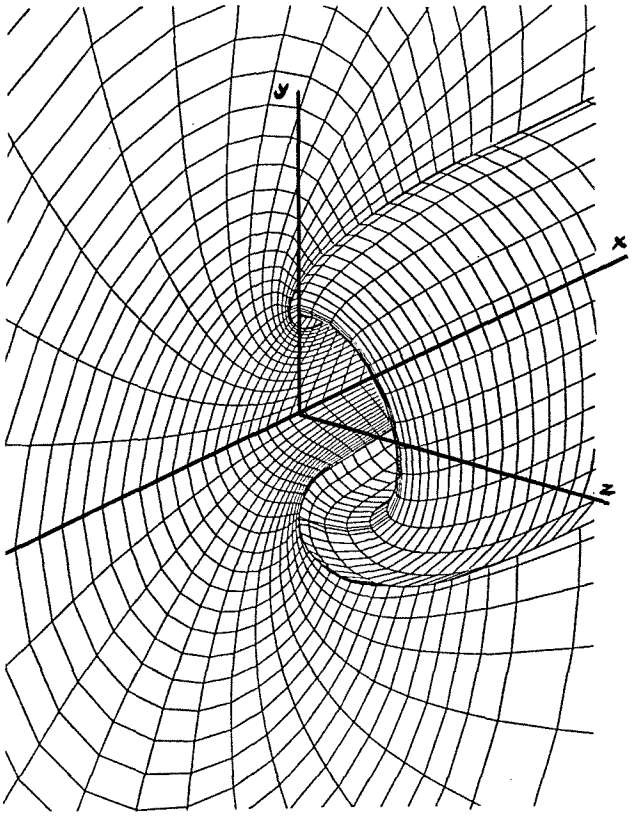

FIG.10: INLET IN SUBSONIC FLOW WITH MAXWELL GRID

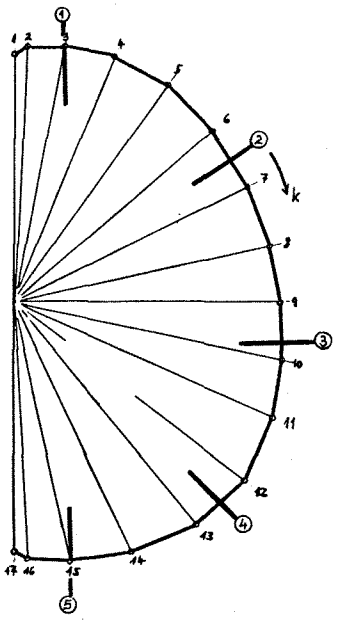

FIG.11: NOSE-POINT LINE, GRID SECTIONS K AND PRESSURE-HOLE STATIONS 1 - 5

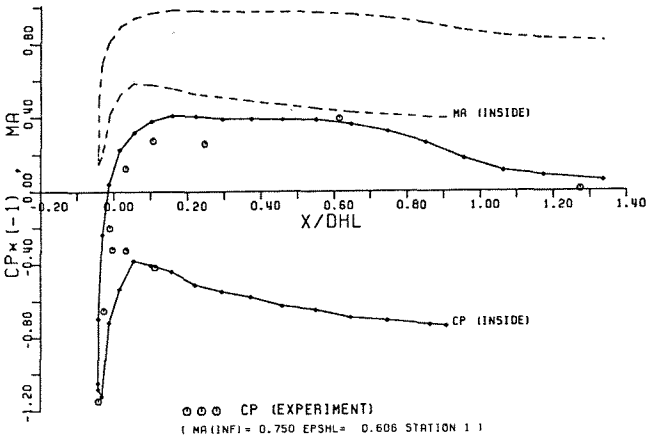

SECTION K= 3

MA(INF)= 0.800 ALPHA= 0.0 PEX= 1.32700 EPSHL= 0.60220 DHL=677.020

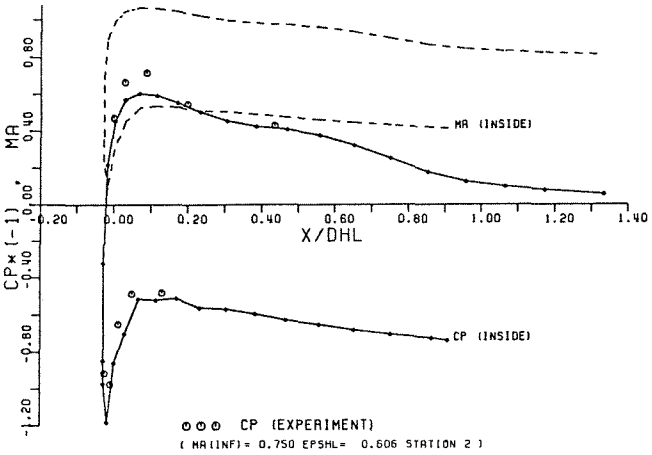

SECTION K= 6

MA(INF)= 0.800 ALPHA= 0.0 PEX= 1.32700 EPSHL= 0.60220 DHL=677.020

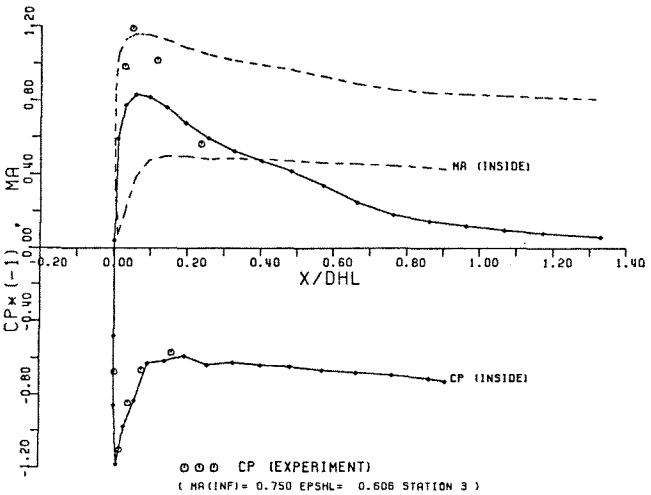

SECTION K= 9

MA(INF)= 0.800 ALPHA= 0.0 PEX= 1.32700 EPSHL= 0.60220 DHL=677.020

FIG.12: COMPARISON OF WALL-PRESSURE DISTRIBUTIONS WITH EXPERIMENT, $\alpha=0^{\circ}$

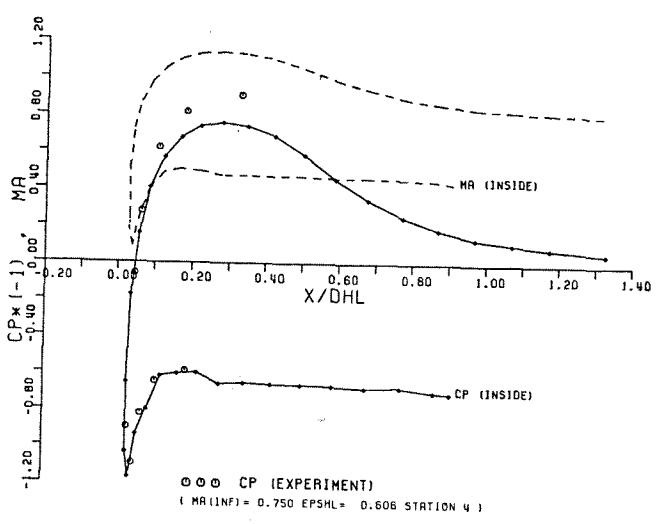

SECTION K=12

MA(INF)= 0.800 ALPHA= 0.0 PEX= 1.32700 EPSHL= 0.60220 DHL=677.020

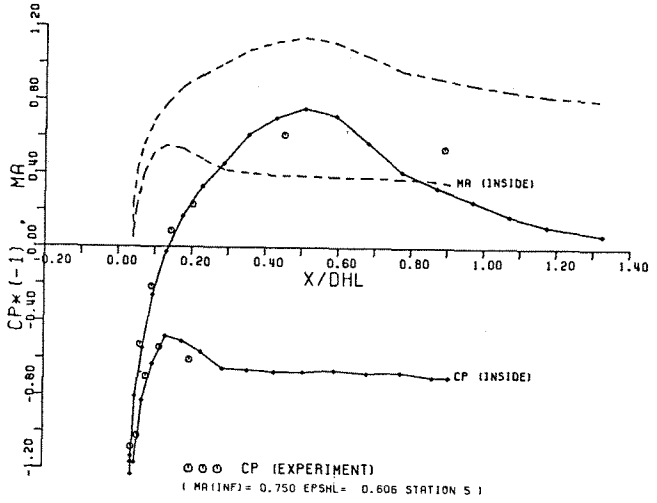

SECTION K=15

MA(INF)= 0.800 ALPHA= 0.0 PEX= 1.32700 EPSHL= 0.60220 DHL=677.020

FIG.12: CONTINUED

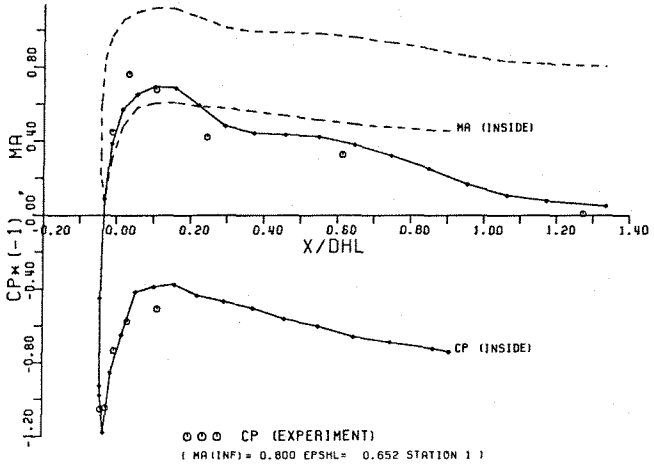

SECTION K= 3

MA(INF)= 0.800 ALPHA= 6.00 PEX= 1.32700 EPSHL= 0.66700 DHL=677.020

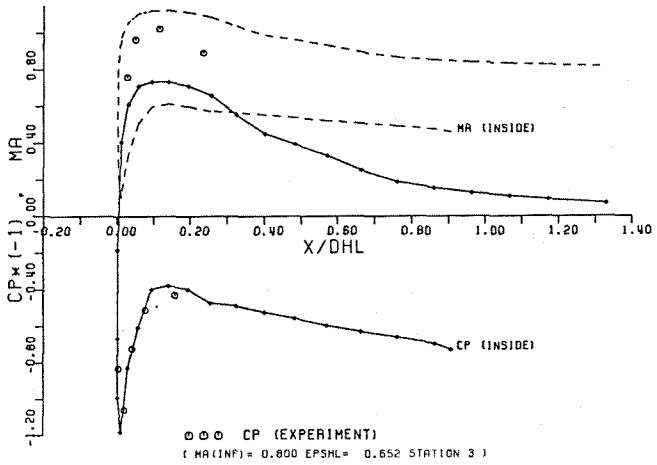

SECTION K= 9

MA(INF)= 0.800 ALPHA= 6.00 PEX= 1.32700 EPSHL= 0.66700 DHL=677.020

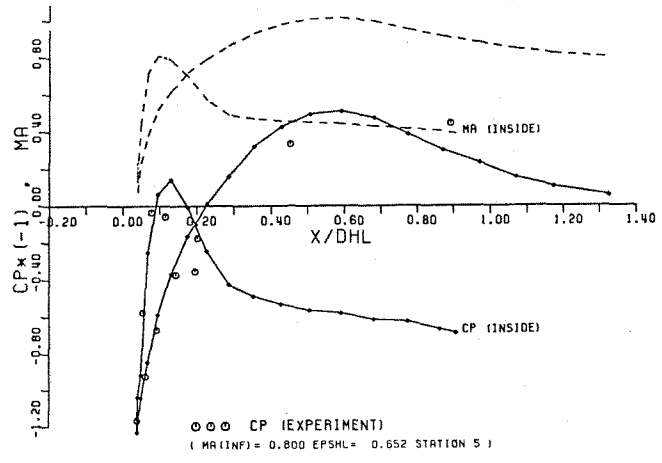

SECTION K=15

MA(INF)= 0.800 ALPHA= 6.00 PEX= 1.32700 EPSHL= 0.66700 DHL=677.020

FIG.13: COMPARISON OF WALL-PRESSURE DISTRIBUTIONS WITH EXPERIMENT, $\alpha = 6°$

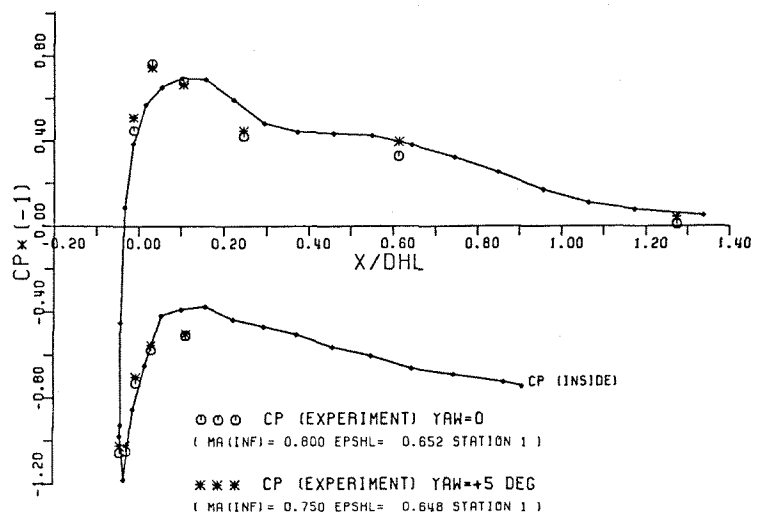

SECTION K= 3

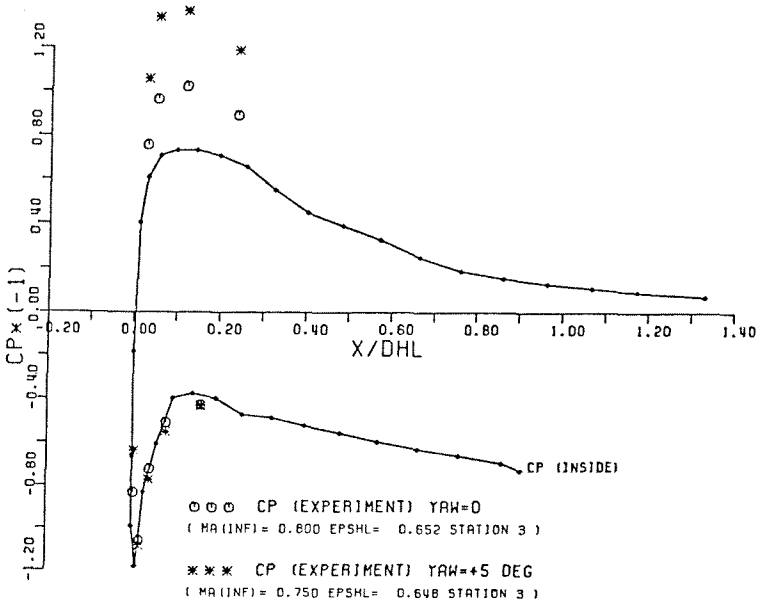

SECTION K= 9

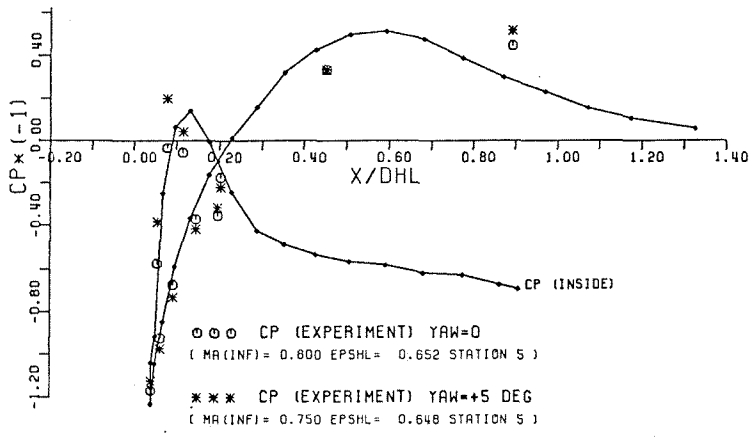

SECTION K=15

FIG.14:

COMPARISON OF WALL-PRESSURE DISTRIBUTION WITH EXPERIMENTS AT YAW=0 AND YAW=5 FOR EXPLANATION OF SUCTION-PEAK DIFFERENCES AT SIDE-SECTIONS OF THE INLET

THEORY: M=0.80, ALPHA=6°, P_{ex}/P_o=1.327, EPSHL=0.667

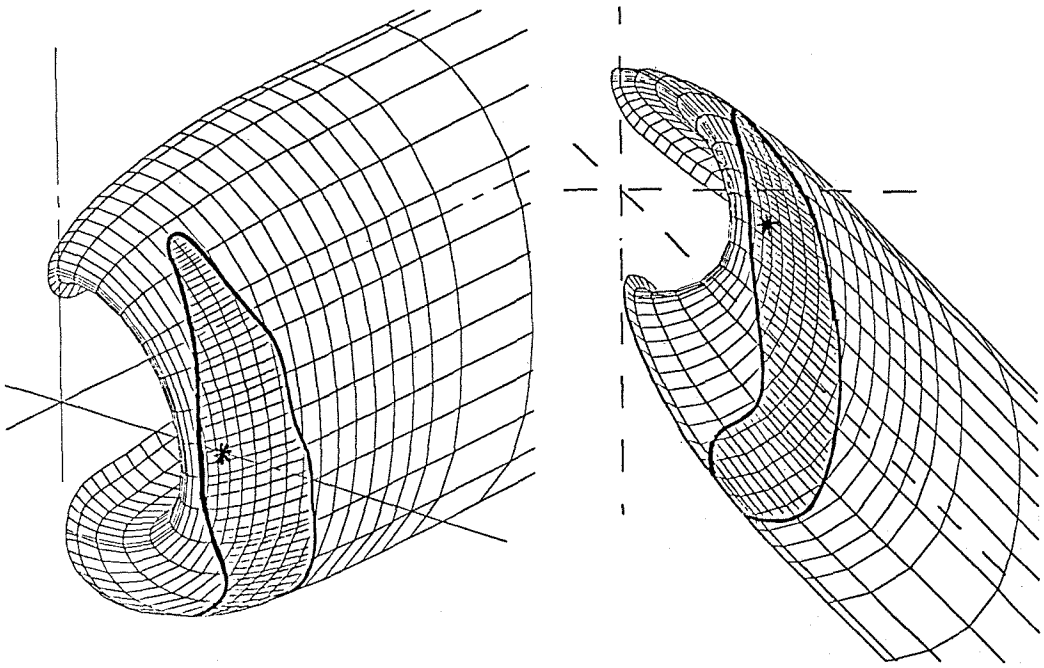

FIG.15: SUPERSONIC FLOW REGION ON INLET SURFACE, ALPHA=0.°

* CELL WITH MAX. MACH-NO. (=1.158)

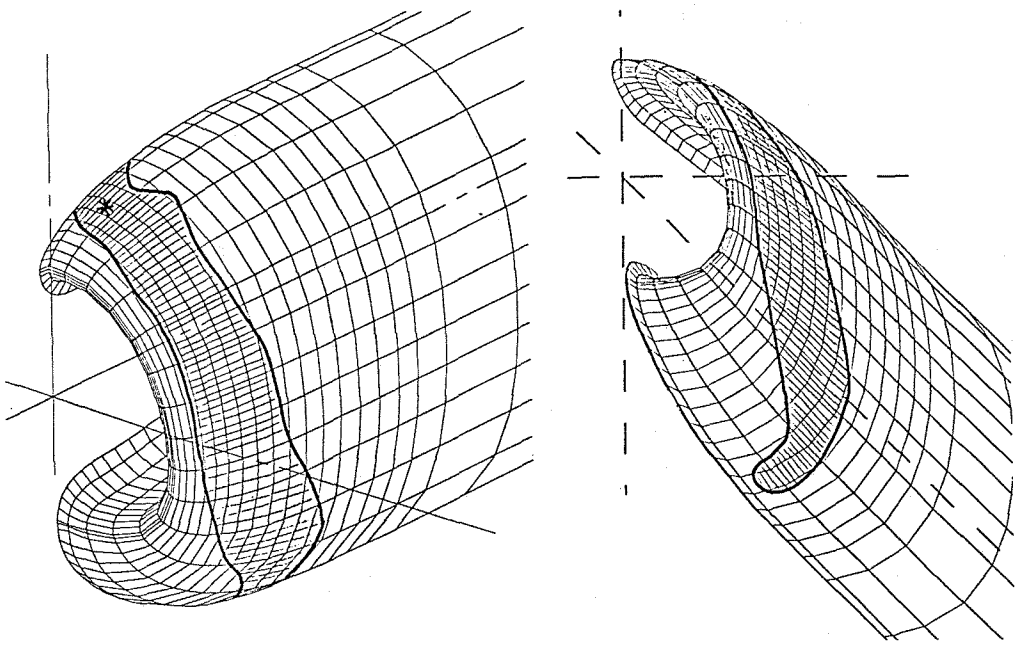

FIG.16: SUPERSONIC FLOW REGION ON INLET SURFACE, ALPHA=6.0°

* CELL WITH MAX. MACH-NO. (=1.163)